Oligomerization of Fusogenic Peptides Promotes Membrane Fusion by Enhancing Membrane Destabilization

Wai Leung Lau,* David S. Ege,[†¶] James D. Lear,* Daniel A. Hammer,[†‡¶] and William F. DeGrado*

*Department of Biochemistry and Molecular Biophysics, School of Medicine; Departments of [†]Chemical and Biomolecular Engineering and [‡]Bioengineering, School of Engineering and Applied Science; and [¶]Institute for Medicine and Engineering, University of Pennsylvania, Philadelphia, Pennsylvania USA

ABSTRACT   A key element of membrane fusion reactions in biology is the involvement of specific fusion proteins. In many viruses, the proteins that mediate membrane fusion usually exist as homotrimers. Furthermore, they contain extended triple-helical coiled-coil domains and fusogenic peptides. It has been suggested that the coiled-coil domains present the fusogenic peptide in a conformation or geometry favorable for membrane fusion. To test the hypothesis that trimerization of fusogenic peptide is related to optimal fusion, we have designed and synthesized a triple-stranded coiled-coil X31 peptide, also known as the ccX31, which mimics the influenza virus hemagglutinin fusion peptide in the fusion-active state. We compared the membrane interactive properties of ccX31 versus the monomeric X31 fusogenic peptide. Our data show that trimerization enhances peptide-induced leakage of liposomal contents and lipid mixing. Furthermore, studies using micropipette aspiration of single vesicles reveal that ccX31 decreases lysis tension, τ_{lysis}, but not area expansion modulus, K_a, of phospholipid bilayers, whereas monomeric X31 peptide lowers both τ_{lysis} and K_a. Our results are consistent with the hypothesis that oligomerization of fusogenic peptide promotes membrane fusion, possibly by enhancing localized destabilization of lipid bilayers.

INTRODUCTION

Membrane fusion reactions are involved in many important biological processes, such as transmission of neurotransmitters across synapses, fertilization, intracellular trafficking, recycling of membrane components, and fusion of enveloped viruses with host cells (Brunger, 2001; Eckert and Kim, 2001; Hernandez et al., 1996; Jahn and Sudhof, 1999; White, 1992). For the most part, lipid bilayers and membranes do not spontaneously achieve contact or fusion because strong electrostatic, hydration, and steric repulsion forces present large energetic barriers (Chernomordik et al., 1987; Helm et al., 1992; Israelachvili et al., 1980; Rand and Parsegian, 1986). In biological systems, these barriers are believed to be overcome by proteins that mediate fusion. To date, many fusion proteins and candidate fusion proteins have been identified (Glabe, 1985; Primakoff et al., 1987; Saginario et al., 1995; Sutton et al., 1998; Trueheart and Fink, 1989; Yagami-Hiromasa et al., 1995).

Of all the fusion systems, the entry of an enveloped virus into the host is considered the simplest membrane fusion reaction because it does not involve mixing of lipid bilayers between distinct subcellular compartments. Thus, it has long been held that the viral entry process may serve as a model system for the more complicated intracellular trafficking processes. Despite dissimilarities among enveloped viruses, viral fusion proteins share a number of common features. Many of them are synthesized as a single polypeptide chain that becomes fusion-capable after it is enzymatically cleaved to create a new amino terminus at the transmembrane subunit (Jones and Risser, 1993; Lamb, 1993; Rodriguez et al., 1987; Rodriguez-Crespo et al., 1995; Wiley and Skehel, 1987). In addition, they contain a short stretch of sequence, also known as the fusogenic peptide, crucial for the fusion process in the membrane-anchored polypeptide chain (Delahunty et al., 1996; Durrer et al., 1995; Harter et al., 1989; Rapaport and Shai, 1994; Schaal et al., 1995). Furthermore, it has been observed that many viral fusion proteins form homotrimers and contain extended triple-helical coiled coils in their central cores (Skehel and Wiley, 1998, 2000). This suggests that the three-stranded coiled-coil architecture is effective at presenting fusogenic sequences in geometries or conformations favorable for initiating membrane fusion.

Hemagglutinin (HA), a transmembrane glycoprotein of the influenza virus, is by far the most studied and best characterized fusion protein. It plays a critical role in the entry of virus into the host and is required for membrane fusion activity. The HA1 subunit mediates binding to cell-surface sialic acid receptor whereas the HA2 subunit is critical for expression of fusion activity. Influenza infection begins when the virus particle binds to the host's cell-surface receptor(s), possibly sialic acid-containing glycoproteins or glycolipids (Skehel and Wiley, 2000; Wiley and Skehel, 1987). Binding of the virus to the cell-surface receptor is followed by internalization of the entire virus via receptor-mediated endocytosis. Inside the endosome, the mildly acidic environment triggers a conformational change in the

HA that subsequently leads to fusion of the virus envelope with the endosomal membrane.

Of all membrane fusion proteins, the ectodomain of HA was the first whose structure was determined to high resolution. Crystal structures have been determined in neutral and mildly acidic pHs for proteolytic fragments of HA, designated BHA and TBHA2, respectively (Bullough et al., 1994; Wilson et al., 1981). These crystal structures show that the proteins are organized into homotrimers. The BHA and TBHA2 fragments are believed to represent the structure of HA in its native and fusion-active state, respectively. In the BHA, the first 20 amino acids at the N-terminus of HA2, also known as the fusogenic peptide, are buried inside the core. Based upon these structures, it has been hypothesized that HA undergoes a conformational rearrangement when in an acidic environment, resulting in the exposure and projection of the fusogenic peptides to the endosomal membrane (Harter et al., 1988, 1989; Pak et al., 1994). Insertion of the exposed fusogenic peptides into the target membrane is believed to be a critical step in fusion. Furthermore, HA does not act in isolation. Ellens et al. showed that association of several HA trimers at the contact site is required in the fusion reaction (Ellens et al. 1990). Similarly, White and co-workers showed that fusion mediated by the influenza virus hemagglutinin involves the cooperative action of at least three hemagglutinin trimers (Danieli et al., 1996). The work of Bentz and of Blumenthal also supports a similar conclusion (Bentz, 2000; Blumenthal et al., 1996). It appears that clustering of fusion proteins at the fusion site serves an important mechanistic role, since oligomerization of viral fusion proteins has been shown to correlate with virus-induced fusion (Freed et al., 1992; Kielian et al., 1996; Wild et al., 1994). It has been proposed that the fusogenic peptides in the HA trimer would bind the target membrane in a threefold symmetric configuration whereas oligomerization of HAs would cause the fusogenic peptides to associate in the target membrane and participate as an assembly in the fusion process (Cohen and Melikyan, 2001).

Soluble protein fragments and synthetic peptides have been widely used as model systems to study the function of individual fusogenic segments of HA. Epand and co-workers demonstrated that HA2 fragments containing the N-terminal fusogenic peptide are capable of inducing vesicle leakage, lipid mixing, and vesicle aggregation, whereas the kinked loop (amino acids numbered 91 to 127 in the HA2 subunit) regulates the pH-dependent fusogenic activities (Epand et al., 1999; LeDuc et al., 2000). Rafalski et al. showed that the X31 wild-type peptide, consisting of the first 20 amino acids at the HA2 N-terminus, exhibits higher levels of phospholipid binding and peptide-induced leakage at mildly acidic pH than at neutral pH, in the same manner as the full-length protein (Rafalski et al., 1991). Moreoever, the X31 wild-type fusogenic peptide has been shown to destabilize lipid bilayers via pore formation and induce spontaneous lysis

(Longo et al., 1997), although a mutated form of this peptide, the Ac-E4K, had been shown to destabilize lipid membrane to failure without stable pore formation at pH below 4.8 (Zhelev et al., 2001). Using the sea urchin bindin B18 and the designed WAE fusion peptides as model systems, Ulrich et al. and Pécheur et al. showed that fusion occurred concomitantly with the formation of peptide oligomers in the membrane-bound state (Pecheur et al., 1999; Ulrich et al., 1999). However, trimerization or high-order oligomerization of fusogenic peptides has not been directly observed in influenza hemagglutinin or other viral fusion proteins.

This study investigates the importance of fusogenic peptide trimer formation in membrane fusion, using the fusogenic peptide derived from hemagglutinin of the X31 strain of influenza as a model system. We created a peptide trimer that incorporates the wild-type X31 fusogenic peptide at the N-terminus of a V_aL_d peptide that self-assembles into a coiled-coil trimer (Ogihara et al., 1997). In this way, the peptide mimics the low-pH trimer form of the native HA fusion peptide. We refer to this novel peptide as coiled-coil X31, or simply ccX31. The membrane interaction properties of this trimeric peptide were studied at neutral and acidic pH and compared to the behavior of monomeric X31 wild-type fusogenic peptide.

MATERIALS AND METHODS

Materials

Amino acids and reagents for peptide synthesis were purchased from NovaBiochem (Darmstadt, Germany). Solvents for peptide synthesis and purification were obtained from Fisher Scientific (Hampton, NH). Sodium acetate, 2-(N-morpholino)ethanesulfonic acid (MES), 3-(N-morpholino)-propanesulfonic acid (MOPS), N-acety-L-tryptophanamide, dimethylsulfoxide (DMSO), sodium chloride, sucrose, and glucose were purchased from Sigma (St. Louis, MO). The lipids used, 1-stearoyl-2-oleoyl-sn-glycero-3-phosphatidylcholine (SOPC), N-4-nitrobenzo-2-oxa-1,3-diazole phosphatidylethanolamine (NBD-PE), 1-stearoyl-2-oleoyl-sn-glycero-3-(phospho-L-serine) (SOPS), and N-(Lissamine Rhodamine B sulfonyl)1,2-dioleoyl-sn-glycero-3-phosphatidylethanolamine (LRh-PE) were obtained from Avantis Polar-Lipids, Inc (Alabaster, AL). Calcein was purchased from Lancaster Synthesis (Pelham, NH).

Peptide synthesis and purification

The peptides were synthesized using standard solid-phase 9-fluorenylmethoxycarbonyl (Fmoc) method on either a Perkin Elmer Applied Biosystems 433A (Foster City, CA) or Milligen 9050 peptide synthesizer (Burlington, MA). The peptides were assembled on PAL™ solid support (Applied Biosystems, Foster City, CA). Following cleavage from the resin with trifluoroacetic acid (TFA) with thioanisole, ethanedithiol, and anisole (90:5:3:2, v/v), the peptides were purified to homogeneity by reverse-phase HPLC using a Vydac C4 column (22 × 250 mm, 15–20 μm particle size). The ccX31 peptide was eluted by means of a linear gradient from 41% to 51% of acetonitrile in 0.1% TFA over 36 min. The X31 peptide was purified using a linear water-acetonitrile/isopropanol/water (3:6:1, v/v) gradient at 0.14% by volume increase per minute of acetonitrile/isopropanol/water (3:6:1, v/v) in the presence of 0.1% (v/v) TFA. The identities of the peptides were confirmed by MALDI-TOF mass spectrometry using a Perspective

Biosystems Voyager DR-RP Biospectrometery Workstation (Applied Biosystems, Foster City, CA).

Circular dichroism

Stock solution of ccX31 was prepared by dissolving the peptide in deionized water/methanol (1:1, v/v). The concentration of peptide was determined by the absorbance at 280 nm in 6 M guanidinium chloride using an extinction coefficient of 5600 cm^{-1} M^{-1} as the peptide contains one tryptophan. Aliquots of the stock solution were transferred into 10 mM sodium acetate and 10 mM MES at pH 5.0, and 10 mM MOPS and 10 mM MES at pH 7.0, respectively. Spectra were recorded at 25°C on an Aviv model 62A DS circular dichroism spectrophotometer (Aviv Instruments, Lakewood, NJ). Far UV-spectra were scanned from 195 nm to 260 nm. Data was collected for every 1-nm interval and averaged for 4 s. Each of the final spectra was the result of averaging four scans. All spectra were baseline corrected. Mean residue ellipticities (MRE) were calculated using the equation MRE $= \theta_{obsd}/10lcn$ where θ_{obsd} is the ellipticity measured in millidegrees, l is the length of the cell in centimeters, c is the peptide concentration in moles per liter, and n is the number of amino acid residues in the peptide. The percent helix content was calculated from the ellipticity measured at 222 nm, using 0 and $-40,000(1 - 2.5/n)$ deg cm^{2}dmol^{-1} as the values for 0 and 100% helix, respectively, where n is the number of amino acid residues (Chakrabartty et al. 1991).

Sedimentation equilibrium

Sedimentation equilibrium was performed with a Beckman Optima XL-I analytical ultracentrifuge (Beckman Coulter). The initial peptide concentration was 30 μM in pH 7.0 and pH 5.0 buffers. The pH 7.0 buffer contained 10 mM MOPS and 10 mM MES, whereas the pH 5.0 buffer contained 10 mM MES and 10 mM sodium acetate, in the presence of 1% (v/v) DMSO. The samples were centrifuged at 40,000 rpm until equilibrium was reached. The association state of the peptide was determined by fitting the data to a single species using the program Igor Pro (WaveMetrics, Lake Oswego, OR). In the curve fitting, the partial specific volume of the peptide and density of solution were assumed to be 0.75 and 1.000, respectively.

Binding of peptide to phospholipid bilayers

Our peptides contain a Trp residue at position 14 from the N-terminus that is highly conserved in all native HA2 sequences. Fluorescence resonance energy transfer between the tryptophan (donor) and fluorescently labeled phospholipid (acceptor) was used to characterize the binding of the peptides with lipid vesicles. Large unilamellar vesicles (LUVs) for this experiment were prepared by nitrogen stream-evaporation of 25 mg/ml chloroform solutions of SOPC and 0.25 mg/ml of NBD-PE in a glass centrifugation tube, followed by hydration in a pH 7.0 buffer (10 mM MES, mM MOPS). Lipid hydration was coupled with six cycles of freezing, thawing, and sonication, except sonication was omitted in the last cycle. Finally, the lipid suspension was extruded five times through a stack of one 1.0 μm and two 0.1-μm pore size polycarbonate filters (Nucleopore Corp., Pleasanton, CA) in a pressure extruder (Lipex Biomembranes, Vancouver, BC). The total lipid concentration in the solution was 2 mM, with 1.4 mol percent of NBD-PE. The vesicles were stored under nitrogen in the dark at ambient temperature. They were used within 24 h. Small unilamellar vesicles were prepared by nitrogen stream-evaporation of 10 mg/ml chloroform solutions of SOPC and 0.25 mg/ml of NBD-PE, followed by redispersion in the pH 7.0 buffer and bath sonication until visual clarity. The total lipid concentration in the stock solution was 4 mM, with 1.4 mol percent of NBD-PE. The vesicles were stored under nitrogen in the dark at ambient temperature before experiments, and they were used within 24 h.

Preliminary lipid binding experiments were conducted using small unilamellar vesicles at ambient temperature. Fluorescence spectra were acquired using an SLM 8100 spectrofluorometer (Jobin Yvon, Edison, NJ), with the excitation wavelength set at 290 nm. Control experiments using N-acety-L-tryptophanamide as the titrant showed that NBD emission did not increase during the titration, indicating that freely soluble tryptophan does not bind to the lipid vesicles. Titration using ccX31 or X31 resulted in increase in NBD emission, indicating binding of the peptides to the lipid bilayers. For experiments at pH 5, the pH 7.0 buffer was acidified using 2% (v/v) acetic acid so that the final concentration of acetic acid was 0.1% (v/v). To obtain the binding isotherm, LUVs were diluted into the pH 7.0 buffer and then titrated with stock solutions of either coiled-coil X31 or X31 in DMSO. In all cases, the final concentration of DMSO was no higher than 2%. Fluorescence spectra were acquired on a PTI QuantaMaster^{TM} C-60 spectrofluorometer (Photon Technology Intenational, Monmouth Junction, NJ), using excitation wavelength at 290 nm. The emission from 300 nm to 560 nm was recorded for every 1-nm interval. The slit widths of the excitation and emission monochromators were set at 1 nm. All the experiments were performed at room temperature with constant stirring. Spectra were corrected for background and dilution. The increase in emission from NBD (acceptor) indicates binding of the peptides to lipid vesicles. Acceptor emissions from 500 nm to 560 nm at different total peptide concentrations were integrated and the ratios of the integrated intensities relative to the intensity with no peptide added were calculated. The ratio was plotted against total peptide concentration. Control experiments using DMSO as the titrant were also conducted.

Peptide-induced leakage of liposome contents

The leakage of liposome contents to the external medium was monitored by the release of calcein encapsulated in lipid vesicles at a self-quenching concentration. Dilution of calcein relieves self-quenching, leading to increase in fluorescence. The sodium salt of calcein (40 mM) was encapsulated in liposomes, buffered with 10 mM MOPS, 10 mM MES, and 40 mM sodium chloride. The LUVs used in the leakage experiments were composed of SOPC/SOPS (99:1 mol %). The LUVs were prepared using the same procedures as described in the lipid binding experiments. Free calcein outside of the vesicles was removed by gel chromatography on Sephadex G-25. Vesicles were eluted with buffer containing 10 mM MES, 10 mM MOPS, and 115 mM sodium chloride at pH 7.0. The total lipid concentration of the eluted LUVs was ~3.0 mM. In the leakage experiments, aliquots of LUV stock solution were diluted into the elution buffer so that the final concentration of lipid was ~98 μM. Upon addition of peptides from a DMSO stock solution to the LUV suspension, leakage of calcein to the external medium was monitored by increase in fluorescence. Fluorescence measurements for these experiments were done using an SLM-8100 spectrofluorometer (Jobin Yvon), with the excitation wavelength set at 490 nm. For each run, the increase in fluorescence emission at 520 nm was followed for 15 min. One hundred percent leakage was established by lysing the vesicles with 20 μL of 0.1% (w/v) Triton X-100 and the intensity before addition of peptide was taken as the baseline. Leakage experiment at each final peptide concentration was repeated for at least three times and the results averaged. For experiments at pH 5.0, the reaction mixture was acidified to the desired pH by mixing 1 part of 2% (v/v) acetic acid to 19 parts of pH 7.0 buffer, before the peptide is added. Control experiments using Coil V$_a$L$_d$ and stirring in the absence of peptide were conducted.

Lipid mixing experiments

Our lipid mixing experiments were based on the fusion assay developed by Struck (Struck et al., 1981). In this work, we used equal concentrations of unlabeled and labeled vesicles diluted into buffer adjusted to the appropriate pH, and monitored the change in donor emission as aliquots of peptides were added to the vesicles. In our experiments, the intensity at 533 nm, predominantly from the NBD (donor), increases relative to that at 590 nm, mainly from Lissamine Rhodamine (acceptor) as the mole percentage of

labeled lipid decreases upon mixing. Three sets of LUV were prepared: SOPC/SOPS (99:1 mol %), SOPC/SOPS/NBD-PE/LRh-PE (97.8:1:0.6:0.6 mol %), and SOPC/SOPS/NBD-PE/LRh-PE (98.4:1:0.3:0.3 mol %). The procedures for preparing LUVs were described above in the binding experiment section. The NBD-PE and LRh-PE were 1 mg/ml chloroform solutions. The concentration of total lipid in each of the three stock solutions of LUV was ~12.8 mM. In our experiments, the final lipid concentration was ~200 μM. Lipid mixing experiments at each final peptide concentration were repeated at least three times and the results averaged. Experimental data were acquired using either a SLM-8100 spectroflurometer (Jobin Yvon) or Aviv ATF-105 spectrofluorometer (Aviv Instruments). The kinetics of lipid mixing was followed for 15 min. The signal was averaged for 1 s and sampled every 5 s. In the experiment, zero percent lipid mixing was defined by the fluorescence intensity before addition of peptide. Percentage of lipid mixing was normalized to fluorescence emission from the doubly labeled LUVs, with 0.3 mol % of each fluorophore. For experiments at pH 5.0, the LUV suspensions were acidified to the desired pH by mixing 1 part of 2% (v/v) acetic acid to 19 parts of pH 7.0 buffer, before the peptide was added. Control experiments using coil-V_aL_d and DMSO were conducted.

Micropipette aspiration

All sucrose and glucose solutions were prepared with deionized water and filtered through 0.2 micron filters. Solution osmotic strengths were measured using a Model 3300 osmometer from Advanced Instruments (Norwood, MA). Vesicles were prepared by electroformation from SOPC and SOPS. Ten microliters of 99.5% SOPC, 0.5% SOPS (mol %) in chloroform (0.5 mg/ml) was deposited on platinum electrodes using a Hamilton syringe. The chloroform was evaporated at room temperature in a vacuum oven for several hours to leave behind a thin film of lipid. Giant unilamellar vesicles (GUVs) were then formed in a 100-mM sucrose solution by the electro-formation method of Angelova et al. (Angelova and Dimitrov, 1986; Angelova et al., 1992). Although vesicles can also be formed by simple thin film rehydration, electroformation method was preferred due to a consistent high yield of GUVs. Micropipettes were made from 1-mm borosilicate glass capillaries using a Kopf Model 730 Pipette Puller (David Kopf Instruments, Tujunga, CA). Each pipette was then forged to create a smooth square tip using a TPI MF-1 microforge (TPI, St. Louis, MO).

Aspiration experiments were performed on a Nikon Diaphot TMD inverted microscope with Hoffman optics, a custom-made microscope stage and Narishige Model WR-6 and MMO-203 micromanipulators (Narishige International USA, East Meadow, NY). In a control chamber containing glucose buffer, a single lipid vesicle was aspirated with a small suction pressure to hold it in the pipette. The pressure was increased and then decreased in a step-wise fashion to gather stress versus strain data for calculating the area expansion modulus (K_a). The measured values of K_a give confirmation of single bilayer membrane structure, as well as provide a baseline for measuring the effect that adsorbed peptide has on the membrane properties.

After the K_a test, the vesicle was inserted into a much larger transfer pipette. The microscope stage was translated to bring this two-pipette assembly into the test chamber. This second chamber contains an osmotically matched buffer and the test peptide in solution. The vesicle is removed from inside the protective transfer pipette, thereby marking the $t =$ 0 exposure time to the peptide solution. Using Hoffman optics and video microscopy, the vesicle diameter, projection length, and lysis were monitored with time and recorded on S-VHS. If lysis did not occur after a predetermined period of testing time, the K_a test was repeated to gain a measure of how the adsorbed peptide affected the material properties of the membrane. During the K_a test, the membrane is stressed until failure, thereby measuring the critical lysis tension in the presence of the peptide. These experiments were repeated at pH 5 and pH 7 with three different peptides: X31, ccX31, and the coiled-coil ("cc") domain alone.

Time and pressure data were captured by a custom time code unit built by R. Waugh and colleagues (University of Rochester, Rochester, NY). These data and videos of the experiments were recorded on S-VHS using a Sony SVO-9500MD video recorder. The resulting videotapes were analyzed using Labview pixel measurement software (National Instruments, Austin, TX) and custom image analysis routines. These data were then analyzed to generate plots of projection length versus time, relative area expansion versus time (a measure of peptide adsorption), as well as whether or not the peptide caused lysis under the test conditions (Evans and Needham, 1987).

RESULTS

The coiled-coil X31 model system

To test the hypothesis that trimerization enhances the activity of fusogenic proteins, we have designed and synthesized a peptide, designated coiled-coil X31 (ccX31), which mimics the hemagglutinin fusogenic peptide in the acidic pH environment. It has the sequence: GLFGAIAGFI[10]ENG-WEGMIDG[20]GGE<u>V</u>EA<u>L</u>EKK[30]<u>V</u>AA<u>L</u>ESK<u>V</u>QA[40]<u>L</u>EKK-<u>V</u>EA<u>L</u>EH[50]G. The first 20 amino acids are derived from the N-terminal residues of influenza hemagglutinin HA2 subunit of the strain X31F/68, also known as the X31 fusion peptide or wt-20 peptide. Residues numbered 22–51 come from the de novo designed coil-V_aL_d three-helix bundle ("a" and "d" positions are underlined). A glycine was inserted between the coil-V_aL_d and X31 sequences to serve as a flexible linker. Our goal is to create a triple-stranded alpha-helical coiled coil to which the N-terminal fusion peptide is attached, resembling the structure of viral membrane fusion ectodomains in their fusion-active state. The peptide was synthesized and purified as described in Materials and Methods.

Circular dichroism

Fig. 1 shows the circular dichroism spectra of ccX31 dissolved in aqueous buffers at pH 7.0 and 5.0 conditions. The spectra indicate that ccX31 has similar helical content in both pHs, as indicated by the mean residue ellipticities at 208
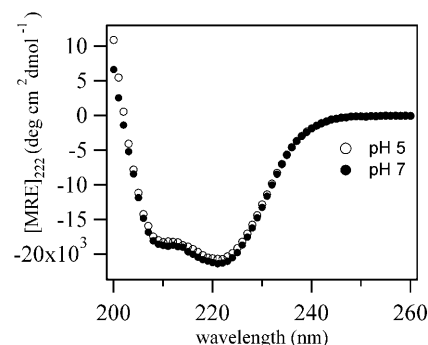

FIGURE 1   CD spectra of ccX31 in pH 5.0 and pH 7.0 buffers. The peptide was added from a concentrated stock solution (~4.1 mM in 50% aqueous methanol) to the buffers to give a final peptide concentration of 53 μM.

and 222 nm. It also shows that the coil-V_aL_d trimerization domain has greatly improved the solubility of the X31 fusogenic sequence so that it can be dissolved in aqueous solution. The observed signals correspond to ~63% helix. Since the coil-V_aL_d region corresponds to about two-thirds of the length of sequence, it implies the X31 fusogenic sequence does not adopt a helix even when it is attached to the coil V_aL_d peptide.

Sedimentation equilibrium

The oligomerization state of the ccX31 was examined using sedimentation equilibrium ultracentrifugation. In aqueous solution at pH 7.0, the peptide associated to form a single homogeneous species with a molecular weight consistent with trimer (Fig. 2). At pH 5.0, the peptide formed higher order aggregates (data not shown).

Peptide binding isotherms

To assess the binding of the peptides to phospholipid vesicles, we used fluorescence resonant energy transfer. The X31 sequence contains a Trp residue, which serves as a fluorescent donor, whereas the LUV contained 1.4 mol % of NBD as a fluorescent acceptor. Binding of the peptide to the NBD-labeled vesicles places the two species in proximity such that excitation of the Trp in the peptide results in an increase in the emission of the NBD. Fig. 3 illustrates the change in fluorescence emission (integrated from wavelength 500 nm to 560 nm) when NBD-labeled LUVs are titrated with increasing concentrations of X31 and ccX31 peptides at ambient temperature. In all cases, fluorescence emission increases as the total peptide concentration is
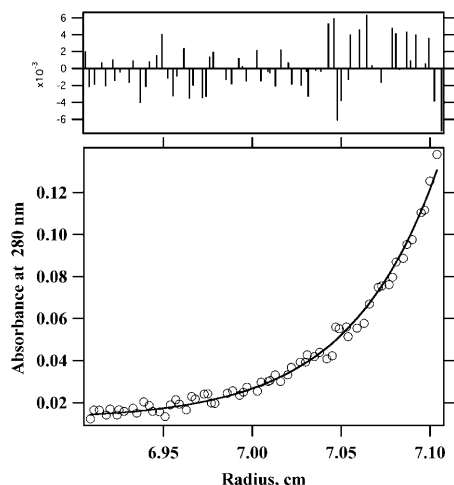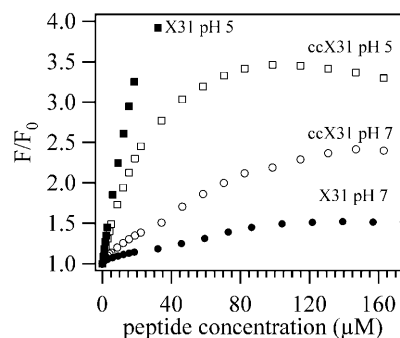
FIGURE 3 Titration of ccX31 and X31 peptides with SOPC/NBD-PE LUV (98.6:1.4 mol %) as monitored by fluorescence. Fluorescence emissions were measured for LUV at 400 μM in buffer with increasing amounts of added peptide, and the intensities in the range of 500–560 nm were integrated. Intensity ratios (F/F_0) are plotted where F_0 is the integrated fluorescence intensity measured in the absence of peptide. ●, X31 at pH 7; ■, X31 at pH 5; ○, ccX31 at pH 7; □, ccX31 at pH 5.

raised. We interpret the increase in fluorescence emission as the result of energy transfer from the tryptophan (donor) on the peptides to the NBD (acceptor) on the lipid. Control experiments using N-acetyl-L-tryptophanamide and DMSO give no increase in fluorescence, indicating that freely soluble tryptophan and DMSO do not modulate the NBD emission. Therefore we conclude that the increase in NBD emission was the result of partitioning of ccX31 and X31 into lipid bilayers. Our binding studies reveal several major observations. First, they show that ccX31 and X31 are able to bind LUVs in both neutral and acidic pH conditions. At pH 7, the increase in fluorescence is larger for ccX31 than X31. This suggests that ccX31 binds more tightly to the vesicle than X31. The higher affinity of ccX31 for lipid can be explained by ccX31's larger cooperative binding units and a smaller loss of entropy upon binding as the fusogenic sequences are preassociated by the coil-V_aL_d trimerization domain. Second, at pH 5, the increase in NBD emission is smaller for ccX31 than X31 at the same peptide concentration range. The apparent higher affinity of X31 for lipid in acidic conditions may be caused by the very low aqueous solubility of X31 at pH 5.0, which would provide a very strong driving force for association with vesicles. Third, we notice that at very low (i.e., a few micromolar) total peptide concentration the binding isotherms appear unresolved for both X31 and ccX31 at both pH 7 and pH 5. We rationalize that a very high lipid-to-peptide ratio favors binding to lipid vesicles because the large excess of lipid provides many high-affinity binding sites for the fusogenic peptides. Under this condition, X31 and ccX31 bind lipid vesicles with similar affinity.

The binding isotherms obtained under neutral pH conditions are multiphasic. For X31, the fluorescence increases linearly with respect to the bulk concentration of peptide up to ~1 μM, corresponding to a lipid-to-peptide ratio of 400. Beyond this point, the binding curve is less

FIGURE 2 (*Bottom panel*) Sedimentation equilibrium analysis of ccX31 in 10 mM MES, 10 mM MOPS at pH 7.0 with 1% (v/v) dimethyl sulfoxide. The loading concentration of ccX31 was ~30 μM. Data collected at 40,000 rpm is shown fitted with trimer species. The top panel shows the residual of the fit.

steep and appears to saturate near 120 μM. Similarly, for ccX31, the fluorescence increases linearly with respect to the bulk concentration of peptide up to ~1 μM, corresponding to a lipid-to-peptide ratio of 400. Beyond this point again, the binding curve is less steep and saturation is reached near 100 μM. This observation can be explained using the scaled-particle approach (Chatelier and Minton, 1996; Minton, 1999; Talbot, 1997; Zuckermann and Heimburg, 2001). This theory allows for the possibility of multiple interconvertible surface conformations, such as interfacially adsorbed, inserted, and pore-forming aggregates, of the membrane-bound proteins, with different affinities. As the total peptide concentration is changed during the titration, the equilibrium distribution among the various species shifts, leading to deviation from classical Langmuir isotherm and the multiphasic appearance of the resulting binding curve. Therefore, we interpret that the initial phase corresponds to binding to the high-affinity sites. Next, a second site with lower affinity for the peptide is populated as the total peptide concentration is raised. These changes give rise to the observed multiphasic profile.

The binding curves obtained at pH 5, however, resemble classical binding isotherms. It is possible that the mildly acidic environment has the effect of increasing the affinities of the peptide for the low-affinity sites rendering it difficult to differentiate from the high-affinity binding sites. An alternative explanation is that the acidic environment favors predominantly one surface state. Consequently the binding isotherms reveal the titration of the major species only. However, it is not possible to unambiguously identify or distinguish the formation of different surface conformations from the changes in fluorescence emission. From the binding isotherms obtained under our experimental conditions, we

establish the following rank order of apparent affinity of the peptide for LUV: X31 in acidic pH > ccX31 in acidic pH > ccX31 in neutral pH > X31 in neutral pH.

Peptide-induced leakage of liposomal contents

Fig. 4, a–d, illustrate the time course for the release of calcein from LUVs, induced by the addition of the X31 and ccX31 peptides. In our experiments, both ccX31 and X31 are more active in acidic pH than neutral pH. However, X31 caused leakage at pH 5 only, whereas ccX31 causes leakage at both pH 5 and pH 7. The final extent of leakage increases with increasing peptide-to-lipid ratio (Fig. 5, a–b). Control experiments using the coil-V_aL_d peptide, i.e., ccX31 without the attached fusion peptide, show that it does not destabilize the vesicles in either acidic or neutral pH (data not shown). The difference between ccX31 versus X31 is most apparent in comparison of the activities at pH 7.0, at concentrations ranging from 0.26 to 2.9 μM. X31 shows no activity whereas ccX31 is effective in causing leakage. This higher activity is consistent with the increased binding of ccX31 versus X31. At pH 5.0, ccX31 was approximately fivefold more active than X31 despite the fact that ccX31 has a lower apparent affinity for LUVs. These observations suggest that trimerization of X31 in the membrane-bound state introduces ''cooperative effect(s)'' in destabilizing lipid bilayers.

Another notable feature of the leakage experiment is that the kinetic traces of content leakage appear to level off at <100% completion, even after a long period of time. Szoka and co-workers previously observed similar behavior with the designed GALA peptide (Parente et al., 1990). Their analysis suggests that GALA-induced leakage occurs as an all-or-none event and requires the number of peptide
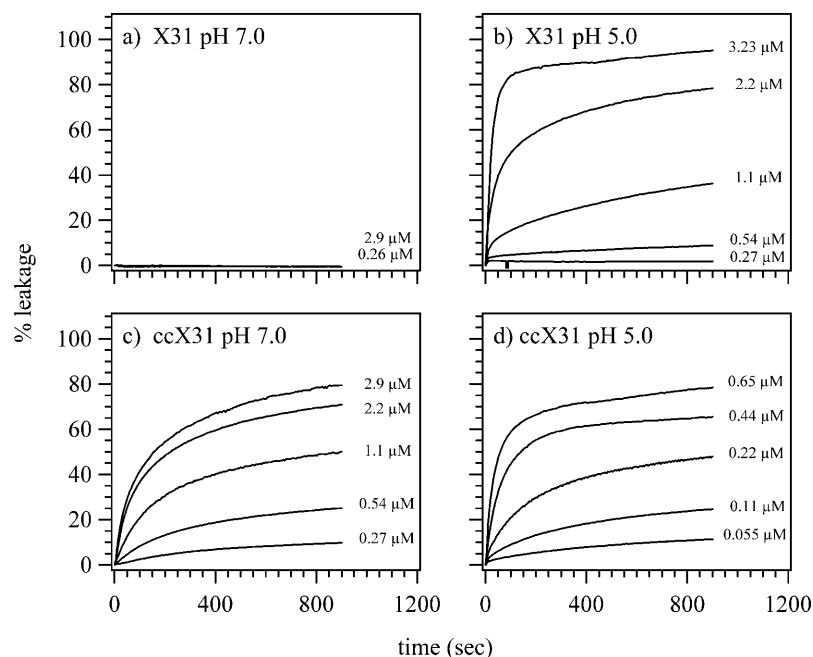

FIGURE 4 Experimental kinetics of calcein release induced by ccX31 and X31. Various amounts of ccX31 and X31 were added to vesicles containing ~40 mM encapsulated calcein in the presence of X31 at pH 7.0 (a), X31 at pH 5.0 (b), ccX31 at pH 7.0 (c), and ccX31 at pH 5.0 (d). The LUVs were composed of SOPC/SOPS (99:1 mol %). The kinetics of the leakage were followed by monitoring the increase of the fluorescence intensity at 520 nm and are plotted versus time.
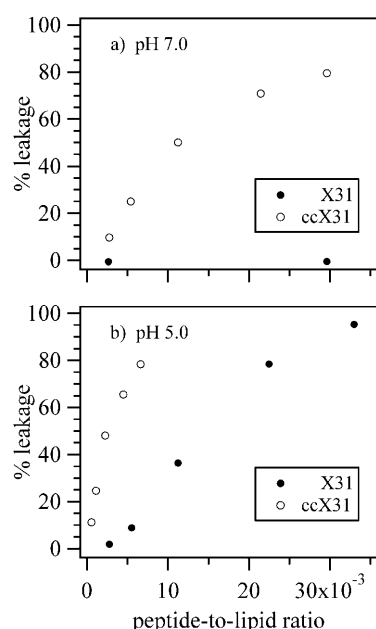
FIGURE 5 Percent calcein leakage from LUV in buffer at 15 min after addition of X31 (●) and ccX31 (○) at pH 7.0 (*a*), and X31 (●) and ccX31 (○) at pH 5.0 (*b*), as a function of peptide-to-lipid ratio. The LUVs were composed of SOPC/SOPS (99:1 mol %).

molecules to exceed certain threshold value. Our results suggest that the mechanisms of X31- and ccX31-induced leakage involve the same requirement. An alternative explanation is that the peptides undergo deactivation as the reaction proceeds and therefore lose their ability to lyse the vesicles.

Peptide-induced mixing of lipid bilayers

Fig. 6, *a–d*, illustrate the mixing of lipid induced by the peptides as a function of time, as indicated by the increase in NBD fluorescence. In our experiment, two populations of vesicles were used, one unlabeled, the other double fluorescently labeled with NBD (donor) and Lissamine Rhodamine (acceptor). Peptide-induced mixing of lipid between these two populations of vesicles will increase the average distance between donor and acceptor in the fused or semifused vesicles. This lowers the energy transfer from the donor to acceptor and leads to an increase in NBD emission. The results of lipid-mixing experiments revealed a pattern similar to those of the leakage experiments. First, X31 is only active at acidic pH, but ccX31 is active at both acidic and neutral pH conditions. Second, ccX31 appears more potent in causing lipid mixing when it is in acidic pH conditions than in neutral pH. Third, both ccX31 and X31 cause measurable rates of lipid mixing at acidic pH, and the final extent of lipid mixing increases with increasing peptide concentration (Fig. 7, *a–b*). Fourth, at pH 5, ccX31 is more active than X31. Finally, the extent of lipid mixing seems to level off at far from complete mixing. Control experiments using the coil-V_aL_d peptide show that it is inactive in both neutral and acidic pHs.

From the binding study, we show that ccX31 and X31 have higher affinities for lipid in acidic pH versus neutral pH. We argue that this observation partly accounts for their stronger abilities to induce lipid mixing in acidic conditions. Similar to the leakage experiment, our data show that, in acidic pH, ccX31 is more effective than X31 in causing lipid mixing even though the binding experiments indicate that ccX31 has a lower affinity for lipid than X31. This suggests
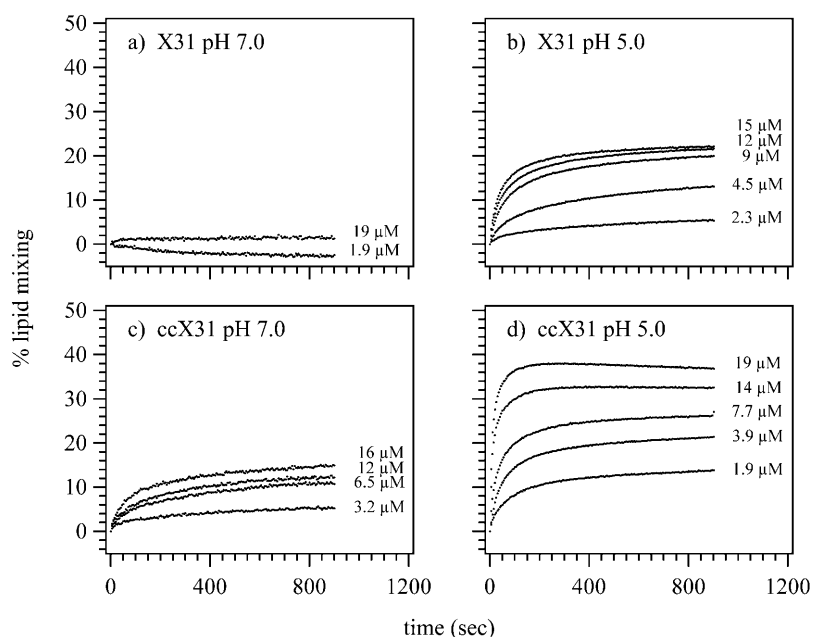

FIGURE 6 Experimental kinetics of lipid mixing induced by ccX31 and X31. Various amounts of ccX31 and X31 were added to vesicles containing ~40 mM encapsulated calcein in the presence of X31 at pH 7.0 (*a*), X31 at pH 5.0 (*b*), ccX31 at pH 7.0 (*c*), and ccX31 at pH 5.0 (*d*). The kinetics of the leakage were followed by monitoring the increase of the fluorescence intensity at 533 nm and are plotted versus time. The unlabeled LUVs and doubly labeled LUVs were composed of SOPC/SOPS (99:1 mol %) and SOPC/SOPS/NBD-PE/LRh-PE (97.8:1:0.6:0.6 mol %), respectively.

FIGURE 7   Percent peptide-induced lipid mixing induced at 15 min after addition of X31 (●) and ccX31 (○) at pH 7.0 (*a*), and X31 (●) and ccX31 (○) at pH 5.0 (*b*), as a function of peptide-to-lipid ratio. The unlabeled LUVs and doubly labeled LUVs were composed of SOPC/SOPS (99:1 mol %) and SOPC/SOPS/NBD-PE/LRh-PE (97.8:1:0.6:0.6 mol %), respectively.
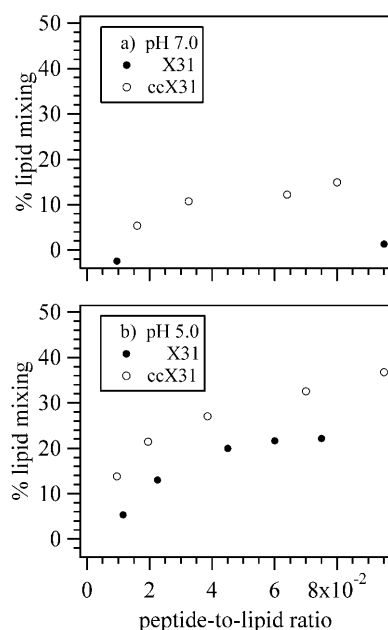
that trimerization of fusogenic peptide enhances lipid mixing. However, it is apparent from the data that the enhancement of lipid mixing is not as striking as in the leakage experiment. The extent of lipid mixing induced by ccX31 at pH 5 is roughly twofold higher than it is at pH 7. Similarly, ccX31 is about twice as potent as X31 in causing lipid mixing in pH 5 solutions. Taking into consideration that ccX31 has a lower affinity for lipid vesicles than X31, as indicated by the binding isotherm, trimerization introduces

only a small degree of cooperative effect in causing lipid mixing.

The correlation between leakage and lipid mixing strongly suggests that lipid mixing involves membrane destabilization. Since the peptide-to-lipid ratios in the lipid-mixing experiments are higher than the corresponding ratios in leakage experiments, it appears that trimerization of the X31 fusogenic sequence enhances membrane destabilization to a higher extent than lipid mixing.

Micropipette aspiration

We focus here on the use of micropipette tests that were developed by Evans and co-workers to measure binding of ccX31 and X31 to lipid vesicles and monitoring the resulting changes in mechanical properties of the lipid bilayers, such as area expansion modulus (K_a) and lysis tension (τ). A glass micropipette was employed to capture and transfer a single GUV from a control buffer into a similar solution containing X31 or ccX31 peptide in solution (Fig. 8). Since our micropipette was connected to a manometer system, the pipette suction pressure applied to the vesicle could be varied precisely using micrometer-driven displacement of a water reservoir. In our setup, the GUVs were suspended in glucose solutions that had a slightly higher osmolarity than the sucrose solution inside the vesicles, therefore they were slightly deflated and had an excess of membrane area (compared to a sphere of the same volume). Under these conditions, the apparent area of the vesicle increases when X31 or ccX31 binds to the vesicle, as indicated by the increase in projection length of the membrane inside the micropipette (Fig. 9). The change of surface area (ΔA) and membrane tension (τ) were determined according to the relationships (Evans and Needham, 1987; McIntosh et al., 1995):
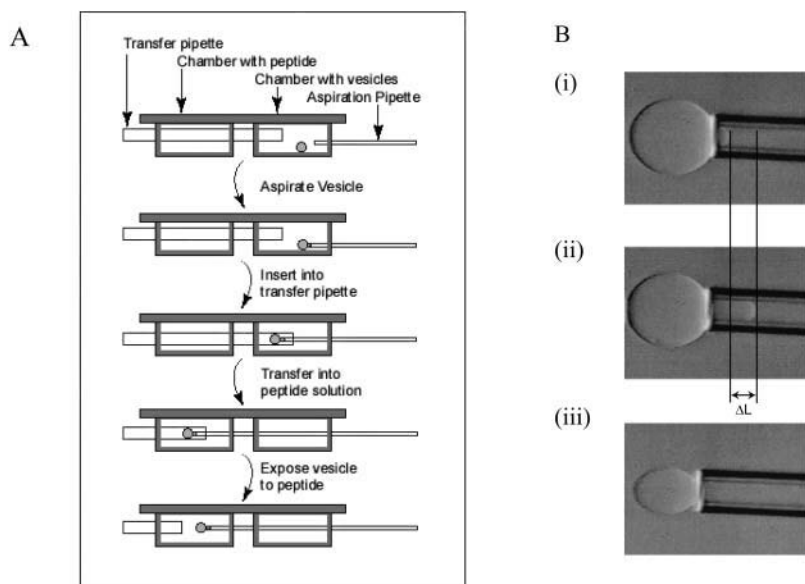

FIGURE 8   (*A*) Schematic of a transfer pipette experiment. Experiments are conducted in glass chambers on the stage of an inverted microscope. (*B*) Photographs of an SOPC vesicle (*i*) before exposure to peptide, (*ii*) increasing projection length due to peptide adsorption, and (*iii*) lysing of vesicle due to peptide.
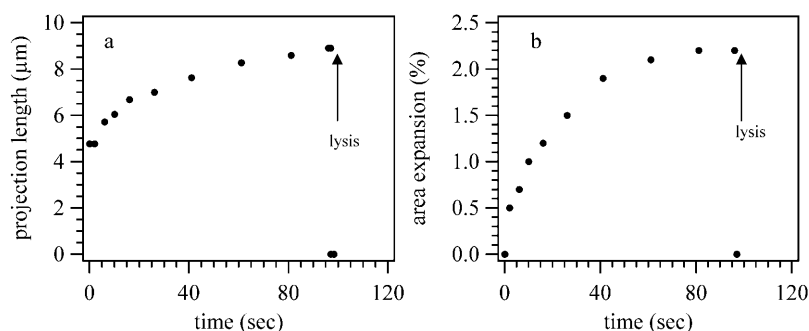
FIGURE 9 Representative aspiration data plots, showing (*a*) change in projection length (*L*) versus time and (*b*) change in area expansion (*α*) versus time for 1 μM ccX31 at pH 5. Note that there is no permeation phase before lysis, which is representative of all experiments with ccX31 at pH 5. If there was a permeation phase after the initial adsorption phase, as seen with the X31 peptide (Longo et al., 1997), then once a pore forms the projection length would begin to decrease as the vesicle swells until it falls. Lysis of the vesicle without the additional strain introduced by swelling indicates that ccX31 induces a dramatic drop in the tension strength of the membrane. The lipid vesicles are SOPC/SOPS (99.5:0.5 mol %).

$$\Delta A = 2\pi R_{\mathrm{p}}(1 - R_{\mathrm{p}}/R_{\mathrm{out}})\Delta L, \quad \text{and}$$

$$\tau = \frac{\Delta P}{2}\left(\frac{R_{\mathrm{out}} * R_{\mathrm{p}}}{R_{\mathrm{out}} - R_{\mathrm{p}}}\right),$$

respectively. In the equations, R_{out} and R_{p} are the radius of the vesicle and pipette, respectively, ΔP is the pipette suction pressure, and ΔL is the change in projection length. We calculated the area expansion, α, using the equation: $\alpha = \Delta A/A_0$ where A_0 is the initial surface area. The area expansion modulus, K_{a}, can be determined from the slope of τ versus α. In the high-tension regime, K_{a} is roughly equal to τ/α (McIntosh et al., 1995).

Our micropipette aspiration experiments confirmed that both ccX31 and X31 are capable of binding to lipid vesicles at pH 5. From the changes in area expansion, we could determine that more X31 binds to the vesicles than ccX31 at pH 5, in agreement with our binding experiments. On average, X31 caused ~4–6% increase in surface area whereas ccX31 caused only 2.3% increase in area. At pH 7, ccX31 caused 0.4% increase in surface area whereas X31 caused no perceptible change in area expansion. Taking all these results together, the extent of peptide binding for GUVs decrease in the order: X31 at pH 5 > ccX31 at pH 5 > ccX31 at pH 7 > X31 at pH 7, agreeing with the fluorescence experiments.

Furthermore, the micropipette experiments revealed that both ccX31 and X31 are capable of perturbing lipid bilayers at pH 5. Control experiments showed that the coil-V$_{\mathrm{a}}$L$_{\mathrm{d}}$ domain caused no lysis or increase in projection length at either pH 5 or 7. At pH 7, in the presence of 1 μM ccX31, ~50% of all vesicles tested lysed. No lysis was detected with X31 at pH 7, even when the peptide concentration was brought to 10 μM. This is an important observation because both peptides adsorbed to the vesicles, but only ccX31 caused lysis at pH 7. At pH 5, both X31 and ccX31 caused lysis of vesicles. However, we should note that the experiments with ccX31 at pH 5 were done at a concentration of 1 μM, a 10-fold lower peptide concentration than with X31 (i.e., 10 μM). In the presence of 10 μM ccX31, lysis of the GUVs was so fast that determination of other aspects of peptide-lipid interaction was not possible. Therefore the ability of the peptide to perturb lipid bilayers decreases in the

order: ccX31 at pH 5 > X31 at pH 5 > ccX31 at pH 7 > X31 at pH 7, agreeing with the fluorescence experiments.

More importantly, the study of single vesicles by micropipette aspiration experiments provides us additional information and insights into the mechanism by which peptides disrupt membranes since such data are difficult to obtain using the bulk experiments. We noticed that exposing a vesicle to a pH 5 solution containing X31 at 1–10 μM caused the projection length (*L*) of the vesicle in the pipette to increase (Longo et al., 1997). Upon reaching a maximum, the projection length decreased until lysis occurred and the vesicle was slowly aspirated into the pipette (Fig. 10). We interpreted the sequence of events as follows. Binding/insertion of the peptides into the vesicle increases the total surface area of the bilayers and therefore the projection length. Then, during the permeation phase, formation of a stable, size-selective pore causes diffusion of glucose due to the chemical potential gradient across the bilayer and cotransport of water into the vesicle due to osmosis, thereby swelling the
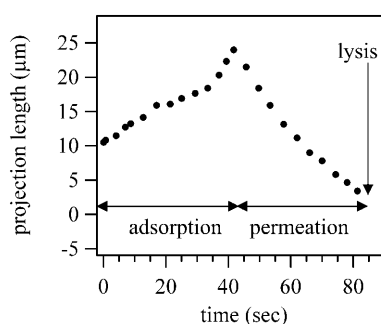

FIGURE 10 Representative projection length (*L*) versus time data for 10 μM X31 at pH 5 (data courtesy of M. Longo). Note the characteristic shape of the curve, compared to that of ccX31 (Fig 9 *a*). First there is an increase in *L* as peptide adsorbs and inserts into the membrane, slightly increasing the apparent surface area of the vesicle. Then, when one or more pores form, there is a transition to the permeation phase. The vesicle swells as glucose and water flow into the vesicle and the larger entrapped sucrose cannot flow out. The projection length decreases as the vesicle swells until failure. This permeation phase is not seen in the ccX31 data. In the presence of ccX31, vesicles lyse without the additional strain introduced by swelling, indicating that ccX31 induces a dramatic drop in the tensile strength of the membrane.

vesicle. Finally, stretching of the lipid bilayers beyond a critical value led to failure of the vesicle membrane.

With ccX31, the projection length L increases to a point and then the vesicle simply lyses, without any apparent permeation phase. Since the applied tension holding the vesicle in the pipette does not change, this implies that the membrane is destabilized to a point that the critical lysis tension falls below the holding tension. This destabilization could be local, or isotropic.

To explore this potential difference in the mechanism of membrane destabilization, we measured the area expansion modulus (K_a) and lysis tension (τ_{lysis}) before and after exposure of the vesicles to the peptides (Table 1). There was a notable difference in behavior between ccX31 and X31. Adsorption of 10 μM X31 decreased K_a at both pH 5 and pH 7, by ~40–50% and 20–35%, respectively. Lysis tension did not decrease at pH 7 after X31 was adsorbed, but it went down 40–60% at pH 5. This is compatible with the observation that X31 has a higher affinity for the membrane at pH 5, and it only causes lysis at pH 5. On the contrary, 1 μM ccX31 did not show any measurable change in K_a at either pH (note the 10-fold lower concentration than X31), yet it reduced the lysis tension by 15–30% at pH 7 and presumably by an even greater extent at pH 5. In our experiments, postexposure K_a tests and lysis tension measurements of ccX31 at pH 5 could not be performed because all of the vesicles lysed spontaneously under those conditions.

DISCUSSION

The findings of this paper provide new information concerning fusogenic peptide/phospholipid vesicle interaction and the contribution of the oligomerization domain to the fusion process. Control experiments using coil-V_aL_d demonstrated that it does not bind to or perturb the lipid bilayers. This finding agrees with our expectation, because coil-V_aL_d self-associates in aqueous solution to form a three-stranded coiled coil, with a transition midpoint of ~0.31 μM (Boice et al., 1996) and solubility in water >20 mg/mL (Ogihara et al., 1997). Thus, the partitioning of the coil-V_aL_d

TABLE 1 Change in area expansion modulus (K_a) and lysis tension (τ_{lysis}) for SOPC vesicles in the presence of X31 and ccX31 peptides, relative to peptide-free measurements

Peptide	pH	Conc (μM)	K_a (mN/m)	τ_{lysis} (mN/m)
				Percent change
ccX31	5	1	n/a	↓ >60%
ccX31	7	1	n/c	↓ 15–30%
X31	5	5	n/c	↓ 25–40%
X31	5	10	↓ 40–50%	↓ 40–60%
X31	7	10	↓ 20–30%	n/c

In the absence of peptide, K_a and τ_{lysis} for SOPC are 193 mN/m (Evans and Rawicz, 1990) and 7.0 ± 0.4 mN/m (Olbrich et al., 2000; Rawicz et al., 2000), respectively. n/c = no change; n/a = not available, i.e., all vesicles lysed spontaneously, so K_a tests were not possible after exposure to peptide.

peptide into lipid bilayers should be negligible. Our findings are consistent with the results reported by Durrer et al. (1996) that binding of HA to lipid bilayers is mediated through the fusogenic sequence but not the coiled-coil region of HA and the observation by Yu et al. (1994) that GCN4 coiled coil does not interact with lipid vesicles. The lipid binding and membrane perturbing properties of X31 exhibit a strong dependence on pH. X31 is fusogenic at acidic pH. At neutral pH, however, it has a greatly impaired ability to bind lipid, cause leakage of contents from liposomes, or induce mixing of lipids. This strong dependence of surface activities on pH has been previously observed (Lear and DeGrado, 1987; Longo et al., 1997; Zhelev et al., 2001). We hypothesize that charge repulsion among Glu[11], Glu[15], and Asp[19] in the X31 will be partially relieved, as they become protonated upon lowering of pH. The attenuation of charge repulsion will favor the formation of amphipathic helix and hence increase the partition at a lipid/water interface. On the other hand, with ccX31, these properties have much less dependence on pH. Compared with X31, ccX31 has a significantly higher level of surface activity at both pH 7 and pH 5. In the fluorescence and micropipette experiments, we had observed that the affinity of peptide for lipid decreases in the order: X31 in acidic pH > ccX31 in acidic pH > ccX31 in neutral pH > X31 in neutral pH. On the other hand, the ability of the peptides to destabilize lipid bilayers decreases in the order: ccX31 in acidic pH > ccX31 in neutral pH > X31 in acidic pH > X31 in neutral pH. Thus the abilities of the peptides to disrupt membrane is not a simple consequence of their binding to bilayers, but instead appears to depend on the oligomerizatin state of the fusogenic peptides. We argue that the observed cooperative effect is compatible with defect formation via aggregation of membrane-bound fusogenic peptide (Rapaport et al., 1996). If pore formation proceeds through association of surface-adsorbed peptides in monomeric form into aggregates of bound peptides and then into pores formed by one or more aggregates of bound peptides, preassociation of the X31 fusogenic peptides (i.e., ccX31) would favor pore formation that leads to content leakage or lysis. This would explain the higher level of content leakage induced by ccX31, i.e., X31 in a trimeric form, despite the fact that it shares the same fusogenic sequence with X31. Along the same line of reasoning, this might explain the lack of activity of X31 in neutral pH, despite the fact that it binds to the lipid bilayers.

We have shown that the order of surface activities of ccX31 and X31 measured by fluorescence and micropipette experiments agree with each other. More importantly, using micropipette aspiration technique, we are able to study the interaction of fusogenic peptides with single vesicles and gain additional insights. A critical finding of this paper is the correlation of the peptides' abilities to insert into and destabilize lipid bilayers with their effects on the mechanical properties on the bilayers. X31 binds to lipid bilayers to a small extent at pH 7. It causes a moderate decrease (20–30%) in

the area expansion modulus (K_a) but not the lysis tension (τ_{lysis}). No spontaneous lysis of vesicles was detected in the micropipette experiments, and no leakage of liposomal contents or lipid mixing was observed in the bulk. At pH 5, X31 has a higher affinity for lipid, as determined from the larger increase in excess surface area (4–6%). It lowers the K_a and τ_{lysis} by 40–50% and 50–60%, respectively. In the fluorescence experiments, we observed significant amounts of vesicle leakage and lipid mixing. Also, our fluorescence experiments indicated that membrane destabilization requires a minimum number of peptides inserted into the membrane. We attribute the increase in binding and the resulting membrane destabilization to the conformational change in the peptide induced by the change in pH (Han et al., 2001).

The ccX31 peptide does not change the area expansion modulus (K_a) at either pH 7 or 5. It lowers τ_{lysis} by 50% at pH 7 and presumably an even greater amount at pH 5. We should note that, in the micropipette experiment, all vesicles lysed spontaneously in the presence of ccX31 at pH 5, so the lysis tension could not be measured at those conditions. Because of the spontaneous lysis, we can conclude that the lysis tension dropped below the small tension applied by the holding pipette. We have shown that ccX31 does not absorb to vesicles as much as X31 does at pH 5, as indicated by the 2.3% versus 4–6% increase in surface area, respectively. Nevertheless, at pH 5, ccX31 causes a greater reduction in lysis tension and also leads to spontaneous vesicle lysis characterized by the absence of an interim permeation phase with stable pores. In the bulk, we observed that ccX31 has a lower affinity for lipid and yet causes a higher extent of leakage than X31. In other words, although ccX31 binds less extensively to the membrane, it nevertheless has a more dramatic effect on destabilizing the membrane than X31.

Comparing the two peptides, we see that ccX31 causes no change in area expansion modulus (K_a) at either pH, but it does dramatically decrease the lysis tension in both neutral and acidic conditions. In the case of X31, decrease of lysis tension is linked to decrease in K_a. Taken together with the fact that a stable permeation phase is not seen with ccX31, our data suggest that the mechanisms for membrane failure are different for X31 and ccX31. In the case of X31, the understanding is that pores form (either transient or stable) that allow the flux of glucose into the vesicle at a more rapid rate than the efflux of the encapsulated sucrose. Therefore, water flows into the vesicles to equalize the osmotic pressure. This causes the vesicles to swell, visualized by decreasing projection length in the pipette. When the vesicles swell to a point where the membrane tension is greater than the lysis tension of the membrane, the vesicles break. Further experiments could provide insight into the approximate size of the pores formed by substituting larger solutes for glucose until the swelling behavior can no longer be observed. By comparison, the ccX31 vesicles spontaneously fail without a detectable permeation phase. It appears that ccX31 peptide

causes a decrease in the stability of the membrane, such that the low holding tension of the pipette causes the vesicles to lyse. We know from the binding studies that, at pH 5, ccX31 binds to the bilayers to a lesser extent but destabilizes the bilayers to a larger extent than X31. Since ccX31 lowers the τ_{lysis} (lysis tension) without affecting the K_a (area expansion modulus), it appears that ccX31 does not weaken the lipid-lipid interaction on the more global scale. That is, the formation of defect is occurring only at one local part of the membrane, instead of many sites all over the surface of vesicles. Therefore, we hypothesize that trimerization of fusogenic peptides, and possibly also formation of higher order aggregates of the ccX31, in the membrane-bound state creates localized defects that cause the membrane to fail because the membrane cannot support the defect formed by the peptide. Thus it causes point defects, rather than an isotopic weakening of the membrane. The importance of protein oligomerization, at the level of the whole protien and fusogenic peptide, in the fusion process had been shown for other viral fusion proteins. Our results here are consistent with these studies (Freed et al., 1992; Kielian et al., 1996; Markovic et al., 1998; Pecheur et al., 1999; Ulrich et al., 1999; Wild et al., 1994). More importantly, it suggests a functional role for the oligomerization of fusogenic peptides in the fusion mechanism. Previously, Yu et al. (1994) reported membrane insertion by the HA coiled-coil peptide and proposed a role for the HA coiled-coil domain in facilitating membrane fusion. Future experiments will be directed to investigate the origin of enhancement of fusogenic activities caused by the coiled coil domain. For instance, we might replace the fusogenic sequence in the ccX31 with known fusion-incompetent mutants, and study their fusogenic properties. Also, we would examine the conformational change of ccX31 upon lipid binding by circular dichroism spectroscopy.

CONCLUSION

In this project, we have demonstrated a consistent pattern of enhanced surface activity for ccX31 over X31. The strong correlation between leakage and lipid mixing strongly indicates that both reactions involve membrane destabilization. Our results are consistent with the hypothesis that oligomerization of fusogenic peptides promotes membrane fusion by facilitating membrane destabilization. It also sheds light onto the biological advantages of having the viral proteins responsible for membrane fusion in oligomeric forms. In addition, analysis of micropipette aspiration data suggest that oligomerization of fusogenic peptides promotes localized membrane instability. This offers the advantage of restricting perturbation to the contact site, therefore minimizing potential damage to the host. However, ccX31 appears to enhance leakage to a greater extent than lipid mixing, implying that lipid mixing involves other segments of the HA or processes besides membrane destabilization.

This also implies other regions in the HA should play important roles in promoting the fusion. Our techniques, however, do not allow us to resolve the interaction between the fusogenic peptide and the bilayers at the molecular level. Structural studies using electron microscopy would provide valuable information on that aspect. We have also pointed out in the previous sections that the transmembrane domain of viral fusion proteins is potentially important in the final step of the fusion process. In the future, the contribution of the transmembrane domain would be probed.

REFERENCES

Angelova, M. I., and D. S. Dimitrov. 1986. Liposome electroformation. *Faraday Discuss.* 81:303–311.

Angelova, M. I., S. Soleau, P. Meleard, J. F. Faucon, and P. Bothorel. 1992. Preparation of giant vesicles by external AC electric fields. Kinetics and applications. *Prog. Colloid Polym. Sci.* 89:127–131.

Bentz, J. 2000. Minimal aggregation size and minimal fusion unit for the first fusion pore of influenza hemagglutinin mediated membrane fusion. *Biophys. J.* 78:227–245.

Blumenthal, R., D. P. Sarkar, D. E. Howard, and S. J. Morris. 1996. Dilation of the influenza hemagglutinin fusion pore revealed by the kinetics of individual cell-cell fusion events. *J. Cell Biol.* 135:63–71.

Boice, J. A., G. R. Dieckmann, W. F. DeGrado, and R. Fairman. 1996. Thermodynamic analysis of a designed three-stranded coiled coil. *Biochemistry.* 35:14480–14485.

Brunger, A. T. 2001. Structure of proteins involved in synaptic vesicle fusion in neurons. *Annu. Rev. Biophys. Biomol. Struct.* 30:157–171.

Bullough, P. A., F. M. Hughson, J. J. Skehel, and D. C. Wiley. 1994. Structure of influenza haemagglutinin at the pH of membrane fusion. *Nature.* 371:37–43.

Chakrabartty, A., J. A. Schellman, and R. L. Baldwin. 1991. Large difference in the helix propensities of alanine and glycine. *Nature.* 351:586–588.

Chatelier, R., and A. P. Minton. 1996. Adsorption of globular proteins on locally planar surfaces: Models for the effect of excluded surface area and aggregation of adsorbed protein on adsorption equilibria. *Biophys. J.* 71:2367–2374.

Chernomordik, L. V., G. B. Melikyan, and Y. A. Chizmadzhev. 1987. Biomembrane fusion - a new concept derived from model studies using 2 interacting planar lipid bilayers. *Biochim. Biophys. Acta.* 906:309–352.

Cohen, F. S., and G. B. Melikyan. 2001. Implications of a fusion peptide structure. *Nat. Struct. Biol.* 8:653–655.

Danieli, T., S. L. Pelletier, Y. I. Henis, and J. M. White. 1996. Membrane fusion mediated by the influenza virus hemagglutinin requires the concerted action of at least three hemagglutinin trimers. *J. Cell Biol.* 133:559–569.

Delahunty, M. D., I. Rhee, E. O. Freed, and J. S. Bonifacino. 1996. Mutational analysis of the fusion peptide of the human immunodeficiency virus type 1: identification of critical glycine residues. *Virology.* 218:94–102.

Durrer, P., C. Galli, S. Hoenke, C. Corti, R. Gluck, T. Vorherr, and J. Brunner. 1996. H+-induced membrane insertion of influenza virus hemagglutinin involves the HA2 amino-terminal fusion peptide but not the coiled coil region. *J. Biol. Chem.* 271:13417–13421.

Durrer, P., Y. Gaudin, R. W. H. Ruigrok, R. Graf, and J. Brunner. 1995. Photolabeling identifies a putative fusion domain in the envelope glycoprotein of rabies and vesicular stomatitis viruses. *J. Biol. Chem.* 87:648–652.

Eckert, D. M., and P. S. Kim. 2001. Mechanisms of viral membrane fusion and its inhibition. *Annu. Rev. Biochem.* 70:777–810.

Ellens, H., J. Bentz, F. Mason, F. Zhang, and J. M. White. 1990. Fusion of influenza hemagglutinin-expressing fibroblasts with glycophorin-bearing liposomes: role of hemagglutinin surface density. *Biochemistry.* 29:9697–9707.

Epand, R. F., J. C. Macosko, C. J. Russell, Y.-K. Shin, and R. M. Epand. 1999. The ectodomain of HA2 of influenza virus promotes rapid pH dependent membrane fusion. *J. Mol. Biol.* 286:489–503.

Evans, E., and D. Needham. 1987. Physical properties of surfactant bilayer membranes: thermal transitions, elasticity, rigidity, cohesion, and colloidial interactions. *J. Phys. Chem.* 91:4129–4228.

Evans, E., and W. Rawicz. 1990. Entropy-driven tension and bending elasticity in condensed- fluid membranes. *Phys. Rev. Lett.* 64:2094–2097.

Freed, E. O., E. L. Delwart, G. L. Buchschacher, and A. T. Panganiban. 1992. A mutation in the human immunodeficiency virus type 1 transmembrane glycoprotein gp41 dominantly interferes with fusion and infectivity. *Proc. Natl. Acad. Sci. USA.* 89:70–74.

Glabe, C. G. 1985. Interaction of the sperm adhesive protein, bindin, with phospholipid vesicles. II. Bindin induces the fusion of mixed-phase vesicles that contain phosphatidylcholine and phosphatidylserine in vitro. *J. Cell Biol.* 100:800–806.

Han, X., J. H. Bushweller, D. S. Cafiso, and L. K. Tamm. 2001. Membrane structure and fusion-triggering conformational change of the fusion domain from influenza hemagglutinin. *Nat. Struct. Biol.* 8:715–720.

Harter, C., T. Bachi, G. Semenza, and J. Brunner. 1988. Hydrophobic photolabeling identifies BHA2 as the subunit mediating the interaction of bromelain-solubilized influenza virus hemagglutinin with liposomes at low pH. *Biochemistry.* 27:1856–1864.

Harter, C., P. James, T. Bachi, G. Semenza, and J. Brunner. 1989. Hyrdophobic binding of the ectodomain of influenza hemagglutinin to membranes occurs through the "fusion peptide". *J. Biol. Chem.* 264:6459–6464.

Helm, C. A., J. N. Israelachvili, and P. M. McGuiggan. 1992. Role of hydrophobic force in bilayer adhesion and fusion. *Biochemistry.* 31:1794–1805.

Hernandez, L. D., L. R. Hoffman, T. G. Wolfsberg, and J. M. White. 1996. Virus-cell and cell–cell fusion. *Annu. Rev. Cell Dev. Biol.* 12:627–641.

Israelachvili, J. N., S. Marcelja, and R. G. Horn. 1980. Physical principles of membrane organization. *Q. Rev. Biophys.* 13:121–200.

Jahn, R., and T. C. Sudhof. 1999. Membrane fusion and exocytosis. *Annu. Rev. Biochem.* 68:863–911.

Jones, J. S., and R. Risser. 1993. Cell fusion induced by the murine leukemia virus envelope glycoprotein. *J. Virol.* 67:67–74.

Kielian, M., M. R. Klimjack, S. Ghosh, and W. A. Duffus. 1996. Mechanisms of mutations inhibiting fusion and infection by Semliki Forest virus. *J. Cell Biol.* 134:863–872.

Lamb, R. A. 1993. Paramyxovirus fusion: a hypothesis for change. *Virology.* 197:1–11.

Lear, J. D., and W. F. DeGrado. 1987. Membrane binding and conformational properties of peptides representing the NH2 terminus of influenza HA-2. *J. Biol. Chem.* 262:6500–6505.

LeDuc, D. L., Y.-K. Shin, R. F. Epand, and R. M. Epand. 2000. Factors determining vesicular lipid mixing induced by shortened constructs of influenza hemagglutinin. *Biochemistry.* 39:2733–2739.

Longo, M., A. J. Waring, and D. A. Hammer. 1997. Interaction of the influenza hemagglutinin fusion peptide with lipid bilayers: area expansion and permeation. *Biophys. J.* 73:1430–1439.

Markovic, I., H. Pulyaeva, A. Sokoloff, and L. V. Chernomordik. 1998. Membrane fusion mediated by baculovirus gp64 involves assembly of stable gp64 trimers into multiprotein aggregates. *J. Cell Biol.* 143:1155–1166.

McIntosh, T. J., S. Advani, R. E. Burton, D. V. Zhelev, D. Needham, and S. A. Simon. 1995. Experimental tests for protrusion and undulation pressures in phospholipid bilayers. *Biochemistry.* 34:8520–8532.

Minton, A. P. 1999. Adsorption of globular proteins on locally planar surfaces. II. Models for the effect of multiple adsorbate conformations on adsorption equilibria and kinetics. *Biophys. J.* 76:176–187.

Ogihara, N. L., M. S. Weiss, W. F. DeGrado, and D. Eisenberg. 1997. The crystal structure of the designed trimeric coiled coil coil-VaLd: Implications for engineering crystals and supramolecular assemblies. *Protein Sci.* 6:80–88.

Olbrich, K., W. Rawicz, D. Needham, and E. Evans. 2000. Water permeability and mechanical strength of polyunsaturated lipid bilayers. *Biophys. J.* 79:321–327.

Pak, C. C., M. Krumbiegel, R. Blumenthal, and Y. Raviv. 1994. Detection of influenza hemagglutinin interaction with biological membranes by photosensitized activation of [125-I]iodonaphthylazide. *J. Biol. Chem.* 269:14614–14619.

Parente, R. A., S. Nir, and F. C. Szoka, Jr. 1990. Mechanisms of leakage of phospholipid vesicle contents induced by the peptide GALA. *Biochemistry.* 29:8720–8728.

Pecheur, E. I., J. Sainte-Marie, A. Bienvenue, and D. Hoekstra. 1999. Lipid headgroup spacing and peptide penetration, but not peptide oligomerization, modulate peptide-induced fusion. *Biochemistry.* 38:364–373.

Primakoff, P., H. Hyatt, and J. Tredick-Kline. 1987. Identification and purification of a sperm surface protein with a potential role in a sperm-egg membrane fusion. *J. Cell Biol.* 104:141–149.

Rafalski, M., A. Oritz, A. Rockwell, L. van Ginkel, J. D. Lear, W. F. DeGrado, and J. Wilschut. 1991. Membrane fusion activity of the influenza virus hemagglutinin: interaction of HA2 N-terminal peptides with phospholipid vesicles. *Biochemistry.* 30:10211–10220.

Rand, P. R., and V. A. Parsegian. 1986. Mimicry and mechanism in phospholipid models of membrane fusion. *Annu. Rev. Physiol.* 48:201–212.

Rapaport, D., R. Peled, S. Nir, and Y. Shai. 1996. Reversible surface aggregation in pore formation by pardaxin. *Biophys. J.* 70:2502–2512.

Rapaport, D., and Y. Shai. 1994. Interaction of fluorescently labeled analogues of the amino-terminal fusion peptide of sendai virus with phospholipid membranes. *J. Biol. Chem.* 269:15124–15131.

Rawicz, W., K. C. Olbrich, T. McIntosh, D. Needham, and E. Evans. 2000. Effect of chain length and unsaturation on elasticity of lipid bilayers. *Biophys. J.* 79:328–339.

Rodriguez, J. F., E. Paez, and M. Esteban. 1987. A 14,000-Mr envelope protein of Vaccinia virus is involved in cell fusion and forms covalently linked trimers. *J. Virol.* 61:395–404.

Rodriguez-Crespo, I., E. Nunez, J. Gomez-Gutierrez, B. Yelamos, J. P. Albar, D. L. Peterson, and F. Gavilanes. 1995. Phospholipid interactions of the putative fusion peptide of hepatitis B virus surface antigen S protein. *J. Gen. Virol.* 76:301–308.

Saginario, C., H.-Y. Qian, and A. Vignery. 1995. Identification of an inducible surface molecule specific to fusing macrophages. *Proc. Natl. Acad. Sci. USA.* 92:12210–12214.

Schaal, H., M. Klein, P. Ghermann, O. Adams, and A. Scheid. 1995. Requirement of N-terminal amino acid residues of gp41 for human immunodeficiency virus type 1-mediated cell fusion. *J. Virol.* 69:3308–3314.

Skehel, J., and D. C. Wiley. 1998. Coiled coils in both intracellular vesicle and viral membrane fusion. *Cell.* 95:871–874.

Skehel, J. J., and D. C. Wiley. 2000. Receptor binding and membrane fusioin in virus entry: the influenza hemagglutinin. *Annu. Rev. Biochem.* 69:531–569.

Struck, D. K., D. Hoeksra, and R. E. Pagano. 1981. Use of resonance energy transfer to monitor membrane fusion. *Biochemistry.* 20:4093–4099.

Sutton, R. B., D. Fasshauer, R. Jahn, and A. T. Brunger. 1998. Crystal structure of a SNARE complex involved in synaptic exocytosis at 2.4 A resolution. *Nature.* 395:347–351.

Talbot, J. 1997. Molecular thermodynamics of binary mixture adsorption: A scaled particle theory approach. *J. Chem. Phys.* 106:4696–4706.

Trueheart, J., and G. R. Fink. 1989. The yeast cell fusion protein FUSI is O-glycosylated and spans the plasma membrane. *Proc. Natl. Acad. Sci. USA.* 86:9916–9920.

Ulrich, A. S., W. Tichelaar, G. Forster, O. Zschornig, S. Weinkauf, and H. W. Meyer. 1999. Ultrastructural characterization of peptide-induced membrane fusion and peptide self-assembly in the lipid bilayer. *Biophys. J.* 77:829–841.

White, J. M. 1992. Membrane fusion. *Science.* 258:917–924.

Wild, C., J. W. Dubay, T. Greenwell, T. Baird, Jr., T. G. Oas, C. McDanal, E. Hunter, and T. Matthews. 1994. Propensity for a leucine zipper-like domain of human immunodeficiency virus type 1 gp41 to form oligomers correlates with a role in virus-induced fusion rather than assembly of the glycoprotein complex. *Proc. Natl. Acad. Sci. USA.* 91:12676–12680.

Wiley, D. C., and J. J. Skehel. 1987. The structure and function of the hemagglutinin membrane glycoprotein of influenza virus. *Annu. Rev. Biochem.* 56:365–394.

Wilson, I. A., J. J. Skehel, and D. C. Wiley. 1981. Structure of the haemagglutinin membrane glycoprotein of influenza virus at 3 A resolution. *Nature.* 289:366–372.

Yagami-Hiromasa, T., T. Sato, T. Kurisaki, K. Kamijio, Y. Nabeshima, and A. Fujisawa-Sehara. 1995. A metalloportease-disintegrin participating in myoblast fusion. *Nature.* 377:652–656.

Yu, Y. G., D. S. King, and Y. K. Shin. 1994. Insertion of a coiled-coil peptide from influenza-virus hemagglutinin into membranes. *Science.* 266:274–276.

Zhelev, D. V., N. Stoicheva, P. Scherrer, and D. Needham. 2001. Interaction of synthetic HA2 Influenza fusion peptide analog with model membranes. *Biophys J.* 81:285–304.

Zuckermann, M. J., and T. Heimburg. 2001. Insertion and pore formation driven by adsorption of proteins onto lipid bilayer membrane-water interfaces. *Biophys. J.* 81:2458–2472.